

# PATCHWORK TERRAINS

Luigi Rocca, Daniele Panozzo and Enrico Puppo  
*DISI, University of Genoa, Via Dodecaneso 35, Genoa, Italy*

Keywords: Terrain Modeling, Multiresolution Modeling, Terrain Rendering.

Abstract: We present a radically new method for the management, multi-resolution representation and rendering of large terrain databases. Our method has two main benefits: it provides a  $C^k$  representation of terrain, with  $k$  depending on the type of base patches; and it supports efficient updates of the database as new data come in. We assume terrain data to come as a collection of regularly sampled overlapping grids, with arbitrary spacing and orientation. A multi-resolution model is built and updated dynamically off-line from such grids, which can be queried on-line to obtain a suitable collection of patches to cover a given domain with a given, possibly view-dependent, level of detail. Patches are combined to obtain a  $C^k$  surface. The whole framework can be designed to take advantage of the parallel computing power of modern GPUs.

## 1 INTRODUCTION

Real time rendering of huge terrain datasets is a challenging task, especially for virtual globes like Google Earth and Microsoft Virtual Earth, which may need to manage terabytes of data. Terrains are usually represented as Digital Elevation Maps (DEMs) consisting of collections of grids, which may have different resolutions and different orientations.

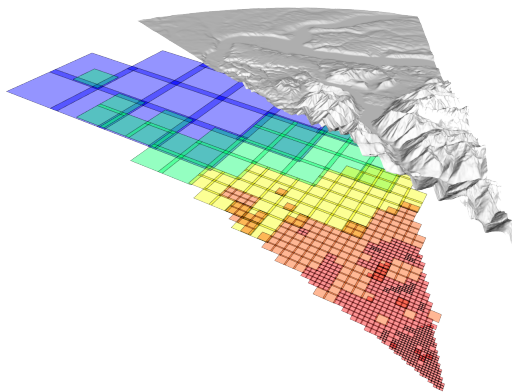


Figure 1: A view-dependent query executed on the Puget Sound Dataset with an on-screen error of one pixel. The different colors represent patches of different sizes.

In order to support interactive rendering, manipulation and computation, it is necessary to adopt approaches that can rapidly fetch a suitable subset of relevant data for the problem at hand. Such a relevant

subset is usually defined in terms of both spatial domain and resolution. Besides view-dependent terrain rendering, specific GIS applications such as analyses in hydrography, land use, road planning, etc., require to handle data at different resolutions. To efficiently support such tasks, a model featuring Continuous Level Of Detail (CLOD) is thus necessary. At the best of our knowledge, all CLOD models in the literature not only require to pre-process the input datasets, but also the data structures they use cannot be updated dynamically with new data (Pajarola and Gobbetti, 2007).

In this paper, we present an approach to CLOD terrain modeling that is radically different from previous literature. Its salient features can be summarized as follows:

1. Our method produces on-line a compact  $C^k$  representation of terrain at the desired accuracy over a given domain. This representation consists of a collection of rectangular patches, of different sizes and orientations, which locally approximate different zones of terrain at different accuracies. Patches can freely overlap and they are blended to obtain a single  $C^k$  function. See Figure 1. The degree of smoothness  $k$  can be selected depending on application requirements.
2. Starting from the input DEMs, we produce a large collection of patches of different sizes and accuracies, and we store them in a spatial data structure indexing a three-dimensional space, having two dimensions for the spatial domain, and a third di-

mension for the approximation error. Every patch is represented as an upright box: its basis corresponds to the domain covered by the patch; its height corresponds to the range of accuracies for which the patch is relevant. We optimize the range of accuracies spanned by each patch, so that the number of patches used to represent a given LOD is minimized. Independent insertion of patches in the spatial index can be performed easily and efficiently, and the result is order independent, thus dynamic maintenance of the database is supported.

3. Spatial queries are executed by finding the set of boxes that intersect a user-defined surface in the space defined above, depending on the desired LOD. Such a surface may be freely defined according to user's needs, thus supporting space culling and CLOD altogether. Incremental queries are possible, so that efficient transfer of patches to the GPU is supported: if the result of a query differs only slightly from the result of the previous one, it is sufficient to transfer to the GPU just the new patches that come in, together with the identifiers of patches to be discarded.
4. The GPU can directly sample this representation to produce an adaptive (possibly view-dependent) tessellation with arbitrary connectivity.

This paper describes the general framework, alongside with two proof-of-concept implementations of our method. The first implementation is tailored for real time rendering: it provides a  $C^0$  representation that can be efficiently sampled in real-time. This representation can be evaluated efficiently in parallel and it is suitable for a GPU implementation. We present results obtained with our CPU implementation, which is already able to support real time rendering (25 fps) on a moderately large dataset (about 256M points) with an error of one pixel in screen space. The second implementation is focused on quality and can be used for common GIS tasks, such as analyses in hydrography, land use, road planning, etc.: it provides a smooth  $C^2$  representation that can support computations on terrain using continuous calculus. Both implementations support CLOD queries.

## 2 RELATED WORK

Overall, known approaches to terrain modeling and rendering can be subdivided in the four categories reviewed in the following. The first category is better suited for modeling purposes, while the other three categories are specifically designed for render-

ing. Our proposal belongs to none of them, and it can be tailored for both rendering, and other GIS tasks, with small modifications to a common framework.

**CLOD Refinement in CPU.** CLOD refinement methods produce triangle meshes that approximate the terrain according to LOD parameters that can vary over the domain (possibly depending on screen or world space error). They are mostly used for modeling and processing purposes, since they provide an explicit representation, with the desired trade-off between accuracy and complexity. Recent surveys on CLOD refinement methods can be found in (Pajarola and Gobbetti, 2007; Weiss and De Floriani, 2010).

**Cluster Triangulations.** Recent GPUs are able to render many millions of triangles per second, so the CPU may spend only a few instructions per triangle in order to prepare data to be rendered in real-time. This fact has led to the development of methods that cluster triangles in a preprocessing steps, possibly at different resolutions, which are then passed to the GPU and rendered in batches. The rendering primitive is not anymore a single triangle, but rather a triangle strip encoding a large zone of terrain. The challenge in these approaches is to stitch different clusters properly. This is usually achieved in a preprocessing step that guarantees conformality of extracted meshes (Cignoni et al., 2003). A survey of these approaches can also be found in (Pajarola and Gobbetti, 2007). They are usually meant exclusively for rendering purposes.

**Geometry Clipmaps.** A different approach has been presented in (Losasso and Hoppe, 2004), where Geometry Clipmaps are stored in the GPU memory, and used to render the part of terrain visible by the user. As the viewpoint moves, the Geometry Clipmaps are updated in video memory. Tessellation is performed directly in the GPU. This method takes advantage of the intrinsic coherence of height maps to compress the input, thus reducing the amount of data that are passed to the GPU. With this method, very high frame rates can be obtained even for huge datasets.

**GPU Ray-casting.** The use of ray-casting for rendering height maps is well studied in the literature, and different GPU techniques that achieve real-time frame rates have been developed in recent years. In (Carr et al., 2006), a method to render meshes represented as Geometry Images is proposed. Following a similar approach, specific methods for real-time

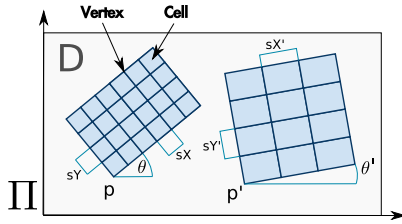


Figure 2: The terrain is covered by a set of regularly sampled grids. Every grid has its own anchor point  $p$ , orientation angle  $\theta$  and different sample steps for the two axes  $sX$  and  $sY$ .

rendering of height maps have been proposed in (Oh et al., 2006; Tevs et al., 2008). However, all these methods were not designed to work with large terrain datasets. In (Dick et al., 2009), a tiling mechanism is used to support real-time rendering on arbitrarily large terrains. Ray-casting methods can be used only for the purpose of rendering, since they do not produce an explicit multi-resolution representation.

### 3 PATCHWORK TERRAINS

In this Section, we describe our technique: in Subsection 3.1, we define the type of patches we use; then, in Subsection 3.2, we describe how patches are blended to form a  $C^k$  representation of terrain; finally, in Subsection 3.3, we describe the multi-resolution model, the order-independent algorithm for the dynamic insertion of patches and the spatial queries.

#### 3.1 From Grids to Patches

We assume a two-dimensional global reference system  $\Pi$  on which we define the domain  $D$  of the terrain, where all input grids are placed. A grid is a collection of regularly sampled height values of terrain. In addition to the matrix of samples, every grid is defined by an anchor point, an angle that defines its orientation, and grid steps in both directions (see Figure 2). In the following, we will use the term *vertex* to denote a sample point on the grid, and the term *cell* to denote a rectangle in  $D$  spanned by a  $2 \times 2$  grid of adjacent vertices. The *accuracy* of a grid also comes as a datum, and it is the maximum error made by using the grid to evaluate the height of any arbitrary point on terrain.

We aim at defining parametric functions that represent small subsets of vertices of the grid, called *patches*. A single patch is defined by an anchor point, its height, its width, and the coefficients that describe the parametric function. For the sake of simplicity, we will consider the height and width of every patch

to be equal, hence the domain of every patch will be a square. Extension to rectangular patches is trivial.

We consider two types of patches: *perfect* patches interpolate the samples of the original terrain; while *approximating* patches only provide an approximation of the original data. We assign an error to each patch, namely the accuracy  $\epsilon$  of the input grid for a perfect patch; and  $\epsilon + \delta$  for an approximating patch, where  $\delta$  denotes the maximum distance between a sample in the input grid and its vertical projection to the patch. We will denote as *kernel* a rectangular region inside every patch, while the rest of the patch will be denoted as its *extension zone*.

The type of function defining a patch, as well as the relation between kernel and extension zones, will vary depending on the application. In Section 4.1 we provide specific examples. Our technique, however, can be used with any kind of parametric function: depending on the application, it may be convenient to use either a larger collection of simpler patches, or a smaller collection of more complex patches. The rest of this section is generic in this respect.

Note that, unlike splines, our patches may freely overlap, without any fixed regular structure.

#### 3.2 Merging Patches

Given a collection of freely overlapping patches, we blend them to produce a smooth function that represents the whole terrain spanned by this collection. In order to obtain a  $C^k$  surface that is efficient to evaluate, we use a tensor product construction, starting from the one dimensional, compactly supported radial basis function defined in (Wendland, 1995). Our weight function is defined as:

$$W(x, y, d) = \frac{w(x/d)w(y/d)}{\int_{-1}^1 \int_{-1}^1 w(x/d)w(y/d) dx dy}$$

for  $x, y \in [-d, d]$  and 0 elsewhere. The 1-dimensional weight  $w(t)$  is a  $C^k$  function with compact support, as defined in (Wendland, 1995): see Figure 3 for the  $C^2$  case and Section 4.1 for further details. It is easy to see that the weight function  $W$  has the following properties:

1. It has compact support in  $[-1, 1] \times [-1, 1]$ ;
2. Its derivatives up to order  $k$  vanish on the boundary of its support;
3. It is  $C^k$  in  $[-1, 1] \times [-1, 1]$ ;
4. It has unit volume.

The first three conditions guarantee that the weight function has limited support, while being  $C^k$

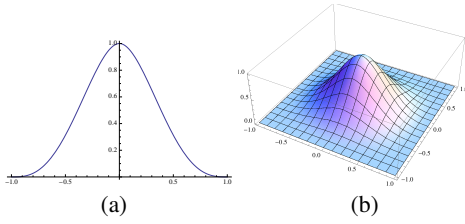


Figure 3:  $C^2$  weight functions: (a) 1D function  $w$ , plotted between -1 and 1. (b) 2D function  $W$ , plotted with  $x,y$  between -1 and 1, with the parameter  $d$  set to 1.

everywhere. This is extremely important for efficiency reasons, as we will see in the following. Property 4 is useful, since it naturally allows smaller (and more accurate) patches to give a stronger contribution to the blended surface.

For every patch  $P$ , we define its weight function  $W^P(x, y)$  as a translated and scaled version of  $W$ , such that its support corresponds with the domain of  $P$ :

$$W^P(x, y) = W(|x - P_x|, |y - P_y|, P_s)$$

with  $P_x$  and  $P_y$  the coordinates of the center of  $P$  and  $P_s$  the size of  $P$ .

A collection of  $C^k$  patches  $P^1, P^2, \dots, P^n$  placed on a domain  $D$ , such that every point of  $D$  is contained in the kernel of at least one patch, defines a  $C^k$  surface that can be computed using the following formula:

$$f(x, y) = \frac{\sum_{i=0}^n P_f^i(x, y) W^{P^i}(x, y)}{\sum_{i=0}^n W^{P^i}(x, y)} \quad (1)$$

with  $P_f^i$  the function associated with patch  $P^i$ .

Note that the surface is  $C^k$  inside  $D$  since it is defined at every point as the product of  $C^k$  functions and the denominator can never vanish since every point in  $D$  belongs to the interior of the domain of at least one patch. The summation actually runs only over patches whose support contains point  $(x, y)$ , since the weight function will be zero for all other patches.

At this point, terrain can be described with an unstructured collection of patches. To use this method on large datasets, we still miss a technique to efficiently compute this representation at a user-defined LOD.

### 3.3 The Multi-resolution Model

We build a multi-resolution model containing many patches at different LODs, and we provide a simple and efficient algorithm to extract a minimal set of patches covering a given region of interest at a given LOD, possibly variable over the domain.

We define a 3D space, called the *LOD space*, in which two axes coincide with those of the global ref-

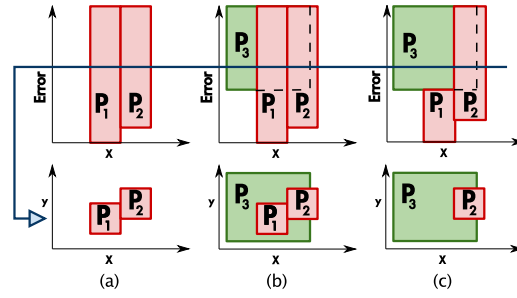


Figure 4: Boxes of patches in LOD space, with a cut shown by the blue line: (a) Two independent patches  $P_1$  and  $P_2$ ; (b) A third patch  $P_3$  is added: patch  $P_1$  becomes redundant for the given cut; (c)  $P_1$  is shortened to obtain a minimal set of patches for every cut of the spatial index.

erence system  $\Pi$ , while the third axis is related to approximation error. For simplicity, we will set a maximum allowed error, so that LOD space is bounded in the error dimension. In this space, every patch will be represented as an upright box (i.e., a parallelepiped), having its basis corresponding to the spatial domain of the patch, and its height corresponding to the range of approximation errors, for which the patch is relevant. The bottom of the box will be placed at the approximation error of the patch, while its top will be set to a larger error, depending on its interaction with overlapping boxes, as explained in the following.

In this section, patches will be always treated as boxes, disregarding their associated functions. We will consider open boxes, so that two boxes sharing a face are not intersecting. For a box  $B$ , we will denote as  $B.min$  and  $B.max$  its corners with minimal and maximal coordinates, respectively. Furthermore for a point  $p$  in LOD space, we will denote its three coordinates as  $p.x$ ,  $p.y$  and  $p.z$ .

Given a collection of patches embedded in LOD space, a view of terrain at a constant error  $e$  can be extracted by gathering all boxes that intersect the horizontal plane  $z = e$ . More complex queries, which may concern a region of interest as well as variable LOD, can be obtained by cutting the LOD space with trimmed surfaces instead of planes.

To informally describe our approach, let us consider the examples depicted in Figure 4. Figure 4(a) shows two non-overlapping patches embedded in LOD space:  $P_1$  is a perfect patch with zero error, and its box extends from zero to maximum error in the LOD space. This means that  $P_1$  will be used to approximate its corresponding part of terrain at all LODs. On the contrary, patch  $P_2$  is an approximating patch: it has its bottom set at its approximation error, while its top is again set at maximum error. Patch  $P_2$  will be used to represent its part of terrain at any error larger or equal than its bottom, while it will not be

used at finer LODs.

In Figure 4(b), a larger patch  $P_3$  is added to our collection, which has a larger error than  $P_1$  and  $P_2$  and also it completely covers  $P_1$ . A cut at an error larger than the error of  $P_3$  would extract all three patches, but  $P_1$  is in fact redundant, since its portion of terrain is already represented with sufficient accuracy from  $P_3$ , which also covers a larger domain. In order to obtain a minimal set of patches, in Figure 4(c) patch  $P_1$  is shortened in LOD space, so that its top touches the bottom of  $P_3$ . Note that we cannot shorten  $P_2$  in a similar way, because a portion of its spatial domain is not covered by any other patch.

This simple example leads to a more complete invariant that patches in LOD space must satisfy to guarantee that minimal sets are extracted by cuts. We first formally describe this invariant, then we provide an algorithm that allows us to fill the LOD space incrementally, while satisfying it. This algorithm builds the multi-resolution model and the result is independent of the order of insertion of patches. Implementation will be described later in Section 4.2.

We define a global order  $<$  on patches as follows:  $P < P'$  if the area of  $P$  is smaller than the area of  $P'$ ; if the two areas are equal, then  $P < P'$  if  $P.min.z > P'.min.z$ , i.e.,  $P$  is less accurate than  $P'$ .

Since both the spatial extension and the approximation error of a patch  $P$  are fixed, the spatial invariant is only concerned with the top of  $P$ , i.e., with its maximal extension in the error dimension.

**Patch Invariant.** A patch  $P$  must not intersect any set of patches, such that the union of their kernels completely covers the kernel of  $P$ , and each patch is greater than  $P$  in the global order  $<$ . Also, the patch  $P$  cannot be extended further from above without violating the previous condition.

In other words, this invariant states that a patch is always necessary to represent terrain at any LOD, in its whole extension in the error domain, because that portion of terrain cannot be covered by larger patches. If all the patches in the model satisfy this property, we are sure that we will obtain a minimal set of patches whenever we cut the model with horizontal planes of the form  $z = c$ . The second part of the invariant forces patches to span all levels of error where their contribution is useful for terrain representation, thus maximizing the expressive power of the model. More general cuts will also extract correct representations in terms of LOD, but minimality is not guaranteed.

Let us consider inserting a new patch  $P$  into a collection of patches that satisfy the invariant. If the new patch does not satisfy the invariant, we shorten it at its top. This is done through Algorithm 1 described below. Note that a patch may be completely wiped out

by the shortening process: this just means that it was redundant. After the insertion of  $P$ , only patches that intersect  $P$  may have their invariance property invalidated, so we fetch each of them and we either shorten or remove it, again by Algorithm 1. All this process is done through Algorithm 2. Shortening patches that were already in the model does not invalidate invariance of other patches, so no recursion is necessary.

---

Algorithm 1: cutter(Patch P, SetOfPatches ps).

---

```

1: sort ps in ascending order wrt min.z
2: current = {}
3: last = {}
4: for P' ∈ ps do
5:   if P ∩ P' then
6:     current = current ∪ {P'}
7:     if the patches in current cover P then
8:       last = P'
9:       break
10:    end if
11:  end if
12: end for
13: if not (last == {}) then
14:   if last.min.z ∩ P.min.z then
15:     Remove P
16:   else
17:     P.max.z = P'.min.z
18:   end if
19: end if

```

---



---

Algorithm 2: add-patch (Patch P).

---

```

1: ps = patches that intersect P
2: cutter(P, ps)
3: for P' ∈ ps do
4:   if P' still intersects P then
5:     ps' = patches that intersect P'
6:     cutter(P', ps')
7:   end if
8: end for

```

---

It is easy to see that all patches in a model built by inserting one patch at a time through Algorithm 2 satisfy the invariant. We also show that the result is independent on the order patches were added.

**Order Independence.** The structure of a model built by repeated application of Algorithm 2 is independent of the insertion order of patches.

**Proof.** The height of the box associated to a patch depends only on the spatial position and minimal error of the other patches inserted in the spatial index. The invariant guarantees that all boxes have their maximum allowed size in the error dimension, with respect

to all other patches in the model. Therefore, the final result only depends on what patches belong to the model.  $\square$

To summarize, the algorithm shown allows us to build a spatial data structure that automatically detects redundant data. Queries are executed by cutting such structure with planes or surfaces. Extracted patches are merged, as explained in Section 3.2, to produce the final terrain representation.

This completes the theoretical foundations of our technique. We discuss the implementation details in Section 4, while we provide benchmarks and results in Section 6.

## 4 IMPLEMENTATION

This section describes a possible implementation of the general framework presented in Section 3, which has been kept as simple as possible for the sake of presentation. In Section 4.1 we describe the construction of patches, while in Section 4.2 we describe the implementation of the spatial index.

### 4.1 Generation of Patches

We describe two types of patches: bilinear patches provides a  $C^0$  representation of the terrain that can be used for rendering purposes; while bicubic patches provide a  $C^2$  representation, trading speed for increased terrain quality.

We use patches at different scales, which are generated from sub-grids of the various levels of a mipmap of terrain data. Each patch is a rectangle that covers a set of samples of the terrains. The patch must represent the terrain it covers, and its size depends on the density of grid samples. Patches may also cover mipmaps, thus allowing to represent larger zones of the terrain with less samples.

For every level of the mipmap, we build a grid of patches such that the union of their kernels form a grid on the domain, and the intersection of their kernel is empty. The size of the kernel with respect to the size of the patch is a parameter controlled by the user, that we denote  $\sigma$ . Any value  $0 < \sigma < 1$  produces a  $C^k$  terrain representation; different values can be used to trade-off between quality and performance: small values of  $\sigma$  improve the quality of blending between patches; conversely, large values reduce the overlapping between different patches, thus improving efficiency, but transition between different patches may become more abrupt, thus producing artifacts. In our experiments, we use  $\sigma = 0.9$ .

**Bilinear Patches.** are formed by a grid of samples and they are simply produced by bilinear interpolation of values inside every  $2 \times 2$  sub-grid of samples. These patches are  $C^0$  in their domain, and the blending function we use is obtained by  $w(t) = (1 - |t|)$ .

**Bicubic Patches.** are formed by a grid of samples, as in the case of bilinear patches. To define a piecewise bicubic interpolating function we compute an interpolant bicubic spline with the algorithm described in (Press et al., 2007). These patches are  $C^2$  in their domain, and the blending function we use is  $w(t) = (1 - |t|)^3(3|t| + 1)$ .

### 4.2 Spatial Index

The spatial index must support the efficient insertion and deletion of boxes, as well as spatial queries, as explained in Section 5.1. An octree would be an obvious choice, but it turns out to be inefficient, because large patches are duplicated in many leaves. We propose here a different data structure that is more efficient for our particular application.

We build a quadtree over the first two dimensions, storing in every node  $n$  (either internal or leaf) the set of patches that intersect the domain of  $n$ . Not all intersecting patches are stored, but just the first  $t$  patches that have their highest value on the  $z$ -axis, and that are not stored in any ancestor node of  $n$ . We use a threshold  $t$  of 64 in our experiments. There is no guarantee that a patch is stored in exactly one node, but in our experiments a patch is always stored in less than two nodes on average.

This data structure can be seen as a set of lists of patches, ordered depending on their highest value on the  $z$ -axis. Such a set is subsequently split into sublists depending on the spatial domain of patches, in a way similar to Multiple Storage Quadtrees (Samet, 2005). A visit of the tree produces an ordered list of the patches that depends only on the spatial domain of the query surface. This list can then be efficiently analyzed to retrieve the patches that intersect the query surface, since it is ordered on a key defined on the third dimension.

Inserting a new box in the tree is simple. Starting at the root, a box  $B$  is inserted in the node(s) that intersects its spatial domain, if and only if either the number of patches in such node does not exceed its capacity, or the highest  $z$ -value of the new box is larger than the highest  $z$ -value of at least another box in the list at that node; in the latter case, the box in the list with the minimum highest  $z$ -value is moved downwards in the tree. Otherwise, the new patch is moved downwards in the tree.

As explained in Section 3.3, queries are specified by a surface in LOD space. The projection of such a surface in the spatial domain is the region of interest (ROI) of the query. The  $z$ -values of the surface define the error tolerance at each point in the ROI. At query time, the quadtree is traversed top-down, and quadrants that intersect the ROI are visited. For each such quadrant, only boxes that intersect the query surface are extracted. When a node  $n$  is visited, the query is propagated to lower levels only if the lowest  $z$ -value of the query surfaces inside the domain covered by  $n$  is less than the highest  $z$ -value of all boxes in  $n$ .

## 5 EXTENSIONS FOR REAL TIME TERRAIN RENDERING

In this Section, we discuss in detail how view-dependent queries can be executed in our framework (Section 5.1) and how our terrain representation is sampled to produce the triangle strip representation used for rendering (Section 5.2).

### 5.1 View-dependent Queries

A view-dependent query is needed to minimize the computational effort required to correctly represent the terrain region of interest. For example, during rendering it is possible to represent with lower resolution areas that are far from viewer, without introducing visual artifacts.

In Section 3.3, a uniform query is executed by cutting the LOD space with a plane parallel to the spatial domain. A view-dependent query is more complex since it involves cutting the spatial index with a more complex surface.

In (Lindstrom et al., 1996) a method was proposed that computes the maximum error in world coordinates that we can tolerate, in order to obtain an error in screen coordinates smaller than one pixel. Such a method defines a surface in LOD space that we could use to make view-dependent queries in our spatial index. However, the resulting surface is complex and the related intersection tests would be expensive. We use an approximation of such a method that allows us to cut the spatial index with a plane, which provides a conservative estimate of the correct cutting surface: we obtain a surface that is correct in terms of screen error, while it could be sub-optimal in terms of conciseness). To compute the cutting plane, we ignore the elevation of the viewer with respect to the position of the point, obtaining the the following formula:

$$\delta_{screen} = \frac{d\lambda\delta}{\sqrt{(e_x - v_x)^2 + (e_y - v_y)^2}},$$

with  $e$  being the viewpoint,  $v$  the point of the terrain where we want to compute the error,  $d$  the distance from  $e$  to the projection plane,  $\lambda$  the number of pixels per world coordinate units in the screen  $xy$  coordinate system,  $\delta$  the error on world coordinate and  $\delta_{screen}$  the error in pixel.

This plane is reduced to a triangle by clipping the zones outside the view frustum. The spatial index is then cut with this triangle, and the intersection between boxes in the index and the triangle are efficiently computed with the algorithm of (Voorhies, 1992), after an appropriate change of reference system has been performed on the box.

### 5.2 Terrain Tessellation

So far, we have shown how to extract a parametric  $C^k$  representation of terrain at the desired LOD. To render the terrain, we rasterize it by imposing a position-dependent grid on the domain and by evaluating the parametric surface only at the vertices of such grid. We produce a grid that has approximately the same number of samples as the number of pixels on the screen, and we define the grid in polar coordinates, thus obtaining a mesh with a high density of vertices in the neighborhood of the viewer and with progressively lower densities as we move farther. For the sake of brevity, we skip the details on the construction of this grid and we focus on the efficient evaluation of the view-dependent terrain representation at its vertices.

Let  $G$  be a grid on the domain of terrain and let  $S$  be a set of patches extracted from the spatial index with a view-dependent query. Equation (1) can be evaluated efficiently by observing that the weight function associated with a patch  $P$  is zero for all the vertices of the grid that lies outside the domain of  $P$ . Thus, for every patch  $P^i$ , we need to evaluate  $P_f^i$  and  $W^{P^i}$  just for the vertices of  $G$  that lie in the domain of  $P^i$ .

We have built a two-dimensional spatial index on the domain on the terrain that contains the position of all vertices of  $G$  and that allows us to rapidly fetch all vertices contained in the domain of a patch. We use a uniformly spaced grid in our prototype. Note that this spatial index has to be built just once, since the grid depends only on the position of the viewer. At each frame, we do not move the grid, but we rather translate and rotate the patches returned by the query to place the grid in the desired position. By using this spatial index, we can efficiently extract the vertices that lie in every patch and incrementally compute Equation (1).

Since the terrain is represented by a parametric

function, it may be also possible to render it efficiently with ray-tracing. We plan to investigate this opportunity as well as other ways to triangulate the parametric representation of the terrain in our future work.

## 6 RESULTS

In this Section we present the results obtained with our prototype implementation on a dataset over the Puget Sound area in Washington. Experiments were run on a PC with a 2.67Ghz Core i5 processor equipped with 4Gb of memory, using a single core. The dataset is made up of  $16,385 \times 16,385$  vertices at 10 meter horizontal and 0.1 meter vertical resolution (USGS and The University of Washington, 2011). Our prototype performs all computation on a single CPU core and achieves interactive rendering frame rates. In a flight over the Puget Sound datasets, our framework obtains an average of 25 fps, producing 320k triangles per frame with an on-screen error of 1 pixel.

As we will show, the majority of time is spent in the rasterization of terrain, which could be parallelized easily on the GPU. If we disable the rasterization, our system is able to respond to hundreds of queries per second. We expect that a GPU implementation, which will be the focus of our future work, will be able to obtain interactive frame rates on large terrains with HD quality, while using only a subset of the cores available on modern GPUs.

Sections 6.1, 6.2, 6.3 and 6.4 present results produced using bilinear patches. Section 6.5 discusses the performance when bicubic patches are used.

### 6.1 Pre-processing time

The preprocessing computations executed by our system can be divided in three phases: mipmap generation, error evaluation and construction of the spatial index. Table 1 reports our preprocessing times for the full dataset, and for two scaled versions. Note that pre-processing is performed online, i.e. it is possible to add new data to a precomputed dataset without the need to rebuild it from scratch. This feature is unique of our method since, at the best of our knowledge, it is not available in any other work in the literature (Pajarola and Gobbetti, 2007).

In our experiments, each patch covers a grid of  $32 \times 32$  samples, while its kernel is made of the central  $28 \times 28$  pixels.

The majority of time is spent on the first two phases, which would be simple to execute in parallel

on multiple cores, unlike the last phase that involves complex data structures.

### 6.2 Space Overhead

On average, our multi-resolution model requires approximately 35% space more than the original dataset. A breakdown of the space occupied by the various components of our model is shown in Table 1. The majority of space is taken by the mipmap.

There is a tradeoff between the space occupied by the multi-resolution model and the size of patches. Smaller patches increase adaptivity but take more space since they must be inserted and stored in the spatial index.

### 6.3 Uniform Queries

Our system is able to execute 800 uniform queries per second with a 50m error. Queries with no error slow down the system to 55 queries per second. Note that the latter queries return the maximum number of patches at the highest level of detail possible.

, yielding the highest number of patches at the most detailed representation possible, can be executed 55 times in a second. Figure 5 shows the results of three different queries performed with an error threshold of 5, 20 and 50 meters. Smaller patches are used to correctly represent fine details, while large patches are used in flat zones, even with a very low error threshold. High frequency detail is obviously lost as error increases.

### 6.4 View-dependent Queries

A single view-dependent query representing a portion of terrain 15km long with an on-screen error of one pixel extracts approximately 250 patches and requires only 2.5ms. Thus, our system is able to query the spatial index at very high frame rates, meaning that the CPU time required for every frame is negligible.

In our prototype, about 95% of the time is spent in evaluating terrain elevations using Equation 1. This task is intrinsically parallel, since it can be performed separately for every vertex of the grid, so we expect to easily obtain impressive frame rates by demanding to the GPU the evaluation procedure. Figure 6 also shows the number of view-dependent queries per second executed by our prototype and the number of extracted patches at different screen error thresholds. The use of progressive spatial queries could further increase performance.

In a GPU implementation of our technique, the query will be executed by the CPU, while the GPU

Table 1: Time and space required to preprocess and store the multi-resolution model. From left to right: the time required to compute the mipmap, to evaluate the error associated with each patch and to build the spatial index; the space required to store the mipmaps, the patches and the spatial index.

Dataset samples	Dataset size	Preprocessing Time				Space overhead			
		Mipmap	Error	Index	Total	Mipmaps	Patches	Index	Total
1k × 1k	2M	0.1s	0.6s	0.05s	0.75s	702k	18k	12k	732k
4k × 4k	32M	0.9s	10s	0.83s	11.73s	11.2M	301k	202k	11.7M
16k × 16k	512M	12.6s	169s	14.6s	196.2s	179M	4.8M	3.2M	187M

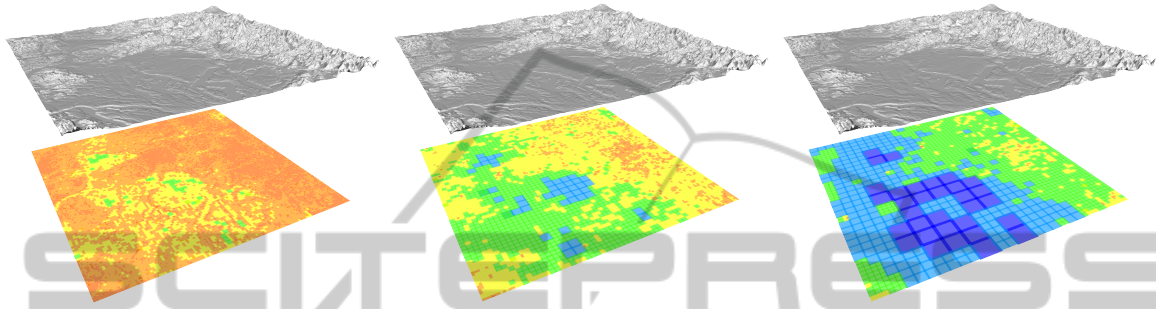


Figure 5: Puget Sound Dataset (16k x 16k samples) rendered with error thresholds of 5, 20 and 50 meters. The colors on the bottom represent the size of the patch used to approximate the terrain. Blue and cyan corresponds to large patches, used to approximate flat zones, while red and orange indicates small patches required to represent fine details.

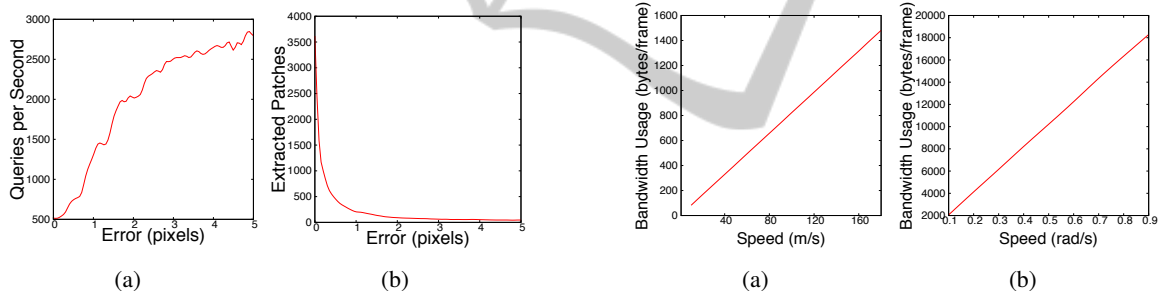


Figure 6: Number of queries per second (a) and number of extracted patches (b) while performing view-dependent queries at different screen error thresholds.

evaluates Equation 1 and rasterizes the resulting terrain. Between different frames, only the difference between the two queries must be sent to the GPU. We have simulated the traffic between CPU and GPU, during a fly over the dataset at different speeds: only a few kb per frame were required to send the difference between two queries to the GPU (see Figure 7). Every patch that has to be sent to the GPU uses 4106 bytes, while the removal of a patch requires only to transfer its unique identifier (4 bytes).

## 6.5 Differences with Bicubic Patches

Changing type of patches influences differently the various steps of our framework. The preprocessing step is slowed down thirty times: this is due to the

Figure 7: During a straight fly over terrain at different speeds, only a few bytes per frame must be sent to the GPU (a). A rotation of the viewpoint requires slightly more bandwidth (b). Both tests were performed with an allowed screen error of three pixels and every query extracted 70 patches on average, representing a portion of terrain 15km long.

huge increase of the computational cost required for the evaluation of the bicubic patches. The construction of the spatial index is almost unaffected by the modification, since the only information that it needs is the maximal error associated with every patch. The space used is similar. The evaluation of the terrain is greatly slowed down and we could obtain just one fps with the CPU implementation. While our current implementation can be used just for modeling purposes, a GPU implementation is required to achieve interactive rendering frame rates with bicubic patches.

## 7 CONCLUDING REMARKS

We have presented a novel technique for representing and manipulating large terrain datasets. Its main advantage is the possibility to efficiently update the system with new heterogeneous grids, a characteristic that is not found in any existing method. The system automatically detects and removes redundant data. Furthermore, our technique produces a multi-resolution  $C^k$  surface instead of a discrete model. The actual evaluation of the surface, which is the only computationally intensive task, can be demanded to the GPU, while keeping the communication between CPU and GPU limited. Texture and normal map can be easily integrated, since they can be associated to every patch and interpolated, with the same method used for the height values.

The space overhead required by the multi-resolution model is approximately the same as the space used for a mipmap pyramid, thus it is suitable to be used even with huge terrains. A limitation of this technique is the lack of a theoretical bound on the maximum number of patches that may overlap at a single point of terrain. This can probably be avoided if we insert additional criteria to the patch invariant we use for building the spatial index, and it will be one of the main points of our future work. However, in our experiments the number of overlapping patches never exceeded six, and it was four on average.

We have presented results obtained with our CPU implementation, which is already able to obtain interactive rendering frame rates using a single core on moderately large terrains. The algorithm for the construction and update of the multi-resolution model, as well as the query algorithms are efficient and capable to manage huge datasets.

We are currently working on a GPU implementation and the most relevant aspects to achieve efficiency are: incremental queries, providing a stream of differences between patches defining terrain in the previous and current frame, which can be directly transferred to the GPU; efficient update of the list of patches maintained in the GPU; and the strategy for parallel evaluation and meshing of terrain.

## REFERENCES

- Carr, N. A., Hoberock, J., Crane, K., and Hart, J. C. (2006). Fast gpu ray tracing of dynamic meshes using geometry images. In Gutwin, C. and Mann, S., editors, *Graphics Interface*, pages 203–209. Canadian Human-Computer Communications Society.
- Cignoni, P., Ganovelli, F., Gobbetti, E., Marton, F., Ponchio, F., and Scopigno, R. (2003). Bdam - batched dynamic adaptive meshes for high performance terrain visualization. *Comput. Graph. Forum*, 22(3):505–514.
- Dick, C., Krüger, J., and Westermann, R. (2009). GPU raycasting for scalable terrain rendering. In *Proceedings of Eurographics 2009 - Areas Papers*, pages 43–50.
- Lindstrom, P., Koller, D., Ribarsky, W., Hodges, L. F., Faust, N., and Turner, G. A. (1996). Real-time, continuous level of detail rendering of height fields. In *SIGGRAPH '96: Proceedings of the 23rd annual conference on Computer graphics and interactive techniques*, pages 109–118, New York, NY, USA. ACM.
- Losasso, F. and Hoppe, H. (2004). Geometry clipmaps: terrain rendering using nested regular grids. In *SIGGRAPH '04: ACM SIGGRAPH 2004 Papers*, pages 769–776, New York, NY, USA. ACM.
- Oh, K., Ki, H., and Lee, C.-H. (2006). Pyramidal displacement mapping: a gpu based artifacts-free ray tracing through an image pyramid. In Slater, M., Kitamura, Y., Tal, A., Amditis, A., and Chrysanthou, Y., editors, *VRST*, pages 75–82. ACM.
- Pajarola, R. and Gobbetti, E. (2007). Survey of semi-regular multiresolution models for interactive terrain rendering. *Vis. Comput.*, 23(8):583–605.
- Press, W. H., Teukolsky, S. A., Vetterling, W. T., and Flannery, B. P. (2007). *Numerical Recipes 3rd Edition: The Art of Scientific Computing*. Cambridge University Press, 3 edition.
- Samet, H. (2005). *Foundations of Multidimensional and Metric Data Structures (The Morgan Kaufmann Series in Computer Graphics and Geometric Modeling)*. Morgan Kaufmann Publishers Inc., San Francisco, CA, USA.
- Tevs, A., Ihrke, I., and Seidel, H.-P. (2008). Maximum mipmaps for fast, accurate, and scalable dynamic height field rendering. In Haines, E. and McGuire, M., editors, *SI3D*, pages 183–190. ACM.
- USGS and The University of Washington (2011). Puget sound terrain. [http://www.cc.gatech.edu/projects/large\\_models/ps.html](http://www.cc.gatech.edu/projects/large_models/ps.html).
- Voorhies, D. (1992). Triangle-cube intersection. *Graphics Gems III*, pages 236–239.
- Weiss, K. and De Florian, L. (2010). Simplex and diamond hierarchies: Models and applications. In Hauser, H. and Reinhard, E., editors, *Eurographics 2010 - State of the Art Reports*, Norrköping, Sweden. Eurographics Association.
- Wendland, H. (1995). Piecewise polynomial, positive definite and compactly supported radial functions of minimal degree. *Advances in Computational Mathematics*, 4(1):389–396.